J Mater Sci: Mater Med (2011) 22:1689–1699
DOI 10.1007/s10856-011-4351-2

Elastomeric electrospun scaffolds of poly(L-lactide-*co*-trimethylene carbonate) for myocardial tissue engineering

Shayanti Mukherjee · Chiara Gualandi · Maria Letizia Focarete · Rajeswari Ravichandran · Jayarama Reddy Venugopal · Michael Raghunath · Seeram Ramakrishna

Received: 2 February 2011 / Accepted: 15 May 2011 / Published online: 27 May 2011

Abstract In myocardial tissue engineering the use of synthetically bioengineered flexible patches implanted in the infarcted area is considered one of the promising strategy for cardiac repair. In this work the potentialities of a biomimetic electrospun scaffold made of a commercial copolymer of (L)-lactic acid with trimethylene carbonate (P(L)LA-*co*-TMC) are investigated in comparison to electrospun poly(L)lactic acid. The P(L)LA-*co*-TMC scaffold used in this work is a glassy rigid material at room temperature while it is a rubbery soft material at 37°C. Mechanical characterization results (tensile stress–strain and creep-recovery measurements) show that at 37°C electrospun P(L)LA-*co*-TMC displays an elastic modulus of around 20 MPa and the ability to completely recover up to 10% of deformation. Cell culture experiments show that P(L)LA-*co*-TMC scaffold promotes cardiomyocyte proliferation and efficiently preserve cell morphology, without hampering expression of sarcomeric alpha actinin marker, thus demonstrating its potentialities as synthetic biomaterial for myocardial tissue engineering.

S. Mukherjee · M. Raghunath
Division of Bioengineering, National University of Singapore, Singapore, Singapore

C. Gualandi · M. L. Focarete (✉)
Department of Chemistry "G. Ciamician" and National Consortium of Materials Science and Technology (INSTM, Bologna RU), University of Bologna, Bologna, Italy
e-mail: marialetizia.focarete@unibo.it

S. Mukherjee · R. Ravichandran · J. R. Venugopal (✉) · S. Ramakrishna
HEM Laboratory, Nanoscience and Nanotechnology Initiative, National University of Singapore, Singapore, Singapore
e-mail: nnijrv@nus.edu.sg

R. Ravichandran · S. Ramakrishna
Department of Mechanical Engineering, National University of Singapore, Singapore, Singapore

M. Raghunath
Department of Biochemistry, Yong Loo Lin School of Medicine, National University of Singapore, Singapore, Singapore

1 Introduction

Myocardial infarction (MI) is the most common cause of death and disability in the developed countries. Current pharmacological and surgical therapies are unable to adequately prevent disease progression. Apart from heart transplantation, there is no standard procedure that can adequately prevent disease progression [1]. Owing to shortcomings of current methods, the search for new strategies to repair the injured myocardium continues. Biomaterial approaches intend to take advantage of the ability of an elastomeric biomaterial sheet to act as a flexible patch sized to fit the infarcted area, while enabling direct apposition of exogenously introduced cells. With this approach, cells would remain intact beneath the patch directly over the infarct site, preventing cell loss and providing a more site-directed repair. Three essential biomaterial criteria include: (i) long term elasticity that matches and responds to the dynamic working conditions of heart muscle; (ii) adaptable biodegradation, which would avoid the detrimental effects of a persisting foreign structure; and (iii) the ability to deliver and retain beating cells at the location of patch attachment [2].

Many efforts by the scientific community in the field of myocardial tissue engineering (MTE) are dedicated to identify materials possessing specific mechanical properties [3]. First of all, it is desirable that the mechanical performances of bioengineered scaffolds match as much as

possible those of the heart extracellular matrix in terms of stiffness, since the scaffold should be flexible enough to promote the contraction of the growing cells [4–6]. In addition, since the myocardial tissue is subjected to cyclical and constant deformation, materials are requested to show elastomeric properties and possibly long-term elasticity.

To date, both natural and synthetic polymers have been proposed as candidates to fabricate three-dimensional (3D) scaffolds for the application in MTE. Since the scaffold should initially act as adhesive substrate for the cells, natural polymers are commonly considered particularly promising. Collagen [7–11], alginate [12–15] and gelatin [16, 17] have been extensively employed in MTE. However, despite the successful results in terms of cell attachment and proliferation, these highly hydrophilic polymers are mainly employed in the form of gels, with limited possibility of designing devices with specific 3D architecture and mechanical properties.

Synthetic elastomeric scaffolds for MTE are desirable as their mechanical conditioning regimens have shown to promote tissue formation along with gradual stress transfer from the degrading synthetic matrix to the newly formed tissue [18, 19]. Synthetic aliphatic polyesters such as polycaprolactone (PCL), poly(glycolic acid) (PGA), poly(lactic acid) (PLA), and their copolymers are popular materials used in the biomedical sector thanks to their clinically confirmed biocompatibility associated with controlled biodegradation rate. They can also be easily processed into 3D structures with defined morphology and thermo-mechanical properties. PGA and PLGA are among the first synthetic biomaterials used for MTE [20–23]. However, the above cited polyesters are generally rigid material under physiological conditions [24]. Biodegradable polyurethanes are another class of synthetic polymers used for MTE that, depending on their chemical structure and macromolecular flexibility, can display an elastic behavior [25–28]. In recent times, new materials for MTE, possessing both suitable mechanical properties and the ability to support cell growth, are developed by following two main approaches: (i) the combination of natural and synthetic polymers, where the natural component is responsible of enhancing cell attachment while the synthetic one acts as the supporting phase with proper mechanical properties [29–31]; (ii) the synthesis of new polymers specifically developed to possess mechanical performances suitable for MTE [3, 32–37].

Co-polymerization is a well known effective approach to synthesize new material with tuned physical properties and controlled hydrophylicity, which in turns determines the rate of hydrolytic degradation. In the context of soft tissue engineering, random copolymers of lactic acid with trimethylene carbonate (PLA-*co*-TMC) have been described as materials possessing attractive thermal and mechanical properties, as well as an interesting hydrolytical degradation behavior. Indeed, by varying the composition of the two co-monomers it is possible to change the polymer thermal and mechanical properties, providing materials that at room temperature range from hard and brittle or moderately tough solids to rubbery and highly elastic solids [38–40]. Porous scaffolds made of P(D,L)LA-*co*-TMC copolymers, obtained by particulate leaching, have been successfully employed by Pego et al. for cardiac tissue engineering [41, 42]. Moreover, when P(D,L)LA-*co*-TMC films were implanted in the back of rats only a mild tissue reaction was observed [43].

In designing scaffolds for MTE, the selection of proper polymeric material must be coupled with a suitable scaffold structure that is capable of mimicking much of the natural extracellular environment. The fibrillar structure of extracellular matrix can be effectively addressed by using electrospinning technique to fabricate micro- and nanofibrous biomimetic porous scaffolds, with interconnected pore structure. Electrospun scaffolds made of synthetic polymers, either coupled with natural polymers or as plain materials, have been used for cardiac tissue engineering in several studies [44–48].

In this study, the potentialities of electrospun P(L)LA-*co*-TMC scaffolds for MTE are presented and discussed for the first time, in comparison with scaffolds of the corresponding homopolymer P(L)LA. A commercial P(L)LA-*co*-TMC copolymer was processed into sub-micrometric fibers by electrospinning and scaffold thermo-mechanical properties were investigated. The capability of the scaffold to act as substrate for cardiomyocyte cell growth was assessed in order to explore the feasibility of engineering a compatible heart patch from P(L)LA-*co*-TMC electrospun fibrous scaffolds.

2 Materials and methods

2.1 Scaffold fabrication

Poly(L-lactide-co-trimethylene carbonate) (P(L)LA-*co*-TMC, Resomer LT 706, LA:TMC 70:30 weight ratio, inherent viscosity 1.2–1.6 dl/g) was purchased from Boheringer Ingelheim, Germany. Poly(L-lactic acid) (P(L)LA, Lacea H.100-E, $M_w = 8.4 \times 10^4$ g/mol, $PDI = 1.7$) was supplied by Mitsui Fine Chemicals (Dusseldorf, Germany). Dichloromethane (DCM) and dimethylformamide (DMF) were purchased by Sigma-Aldrich and were used without any further purification. The electrospinning apparatus, made in house, was composed of a high voltage power supply (Spellman, SL 50 P 10/CE/230), a syringe pump (KD Scientific 200 series), a glass syringe, a stainless-steel

blunt-ended needle (inner diameter: 0.84 mm) connected with the power supply electrode and a grounded aluminum plate-type collector. The polymer solution was dispensed through a Teflon tube to the needle that was vertically placed on the collecting plate. P(L)LA-*co*-TMC solution was prepared at room temperature (RT) by dissolving the polymer in DCM:DMF = 70:30 v/v at a concentration of 12% w/v. P(L)LA-*co*-TMC electrospun scaffolds were fabricated using the following conditions: applied voltage = 16 kV, needle to collector distance = 15 cm, solution flow rate = 0.01 ml/min, at RT and relative humidity RH = 40–50%. P(L)LA scaffolds were fabricated from a solution of P(L)LA in DCM:DMF = 65:35 v/v, at a concentration of 13% w/v, by using the following conditions: applied voltage = 12 kV, needle to collector distance = 15 cm, solution flow rate = 0.015 ml/min, at RT and RH = 40–50%. All the electrospun mats obtained were kept under vacuum over P_2O_5 at RT overnight in order to remove residual solvents.

2.2 Scaffold morphology

SEM observations were carried out by using a Philips 515 SEM at an accelerating voltage of 15 kV, on samples sputter-coated with gold. The distribution of fiber diameters was determined through the measurement of about 250 fibers by means of an acquisition and image analysis software (EDAX Genesis) and the results were given as the average diameter ± standard deviation.

2.3 Scaffold thermal characterization

Thermogravimetric analysis (TGA) measurements were performed with a TA Instruments TGA2950 Thermogravimetric Analyzer from RT to 600°C (heating rate = 10°C/min, nitrogen purge gas). Differential Scanning Calorimetry (DSC) measurements were carried out using a TA Instruments Q100 DSC equipped with the Liquid Nitrogen Cooling System accessory. DSC scans of electrospun scaffolds were performed in helium atmosphere from −50 to 180°C. A rate of 20°C/min was used during heating scans whereas the cooling scans were performed at a rate of 10°C/min. The glass transition temperature (T_g) was taken at half-height of the glass transition heat capacity step, while the crystallization temperature (T_c) and the melting temperature (T_m) were taken at the peak maximum of crystallization exotherm and melting endotherm, respectively.

2.4 Scaffold mechanical characterization

Tensile stress–strain measurements and creep-recovery tests were performed by using a Dynamic Mechanical Thermal Analyzer (DMTA, TA Instruments Q800 series) equipped with tension-film clamps. All the analyses were performed on rectangular strips cut from electrospun mats (width = 5 mm; gauge length = 10 mm). Mat thickness, measured by microcaliper, was: P(L)LA: 23 ± 6 μm; P(L)LA-*co*-TMC: 30 ± 1 μm (about 15 replicate measurements were performed for each sample and results are given as the average value ± standard deviation). Stress–strain measurements were carried out both at RT and at 37°C. In the latter case the sample was heated to 37°C and it was allowed to equilibrate for 5 min prior to beginning the test. Tensile stress–strain measurements were carried out by applying a preload force of 0.001 N and using a cross-head speed of 5 mm/min. Tensile elastic modulus was determined from the initial linear slope of the stress–strain curve. Eight replicate specimens were run for each sample and results were given as the average value ± standard deviation. The creep-recovery measurements were carried out at 37°C. The sample was instantaneously subjected to a stress hold at a constant value for 2 s. After removal of the applied stress the sample recovery was followed for 2 min with no additional force other than the preload force of 0.001 N. The recovery process was monitored by plotting the strain as a function of time.

2.5 Cardiomyocyte isolation and culture

Cardiomyocytes were freshly isolated from adult New Zealand rabbit hearts, as per institution guidelines. The left ventricle of the heart was cleaned thoroughly with Phosphate Buffer Saline (PBS) (1st base) containing antibiotics (Sigma-Aldrich) for removal of fat tissue and clots and it was minced into fine pieces. The processed tissue was treated with 5 mg of collagenase (Sigma-Aldrich) for 20 min at 37°C. Freshly isolated cardiac cells were cultured in DMEM media supplemented with 10% FBS and 1% antibiotic and antimycotic solutions (Invitrogen Corp, USA) in a 75 cm^2 cell culture flask. Cells were incubated at 37°C in a humidified atmosphere containing 5% CO_2 for 6 days and the culture medium was changed every 2 days.

2.6 Scaffold preparation and cell seeding

Each of the nanofibrous scaffolds was adhered to 15 mm coverslip using silicon bioglue and was placed in 24-well plate while being pressed with a stainless steel ring to ensure complete contact of the scaffolds with wells. The specimens were sterilized under UV light, washed three times with PBS and subsequently immersed in complete DMEM overnight before cell seeding. The trypsinised cells from the culture flasks were centrifuged, counted by trypan blue assay using a hemocytometer and seeded onto the scaffolds at a density of 2×10^4 cells/well. These were

allowed to adhere for 3 h before adding medium, which was thereafter changed every 3 days.

2.7 Proliferation study

The adhesion and proliferation of cultured cardiomyocytes on scaffolds and TCP used as control were determined using the colorimetric MTS assay (CellTiter 96 AQueous One solution, Promega, Madison, WI). The reduction of yellow tetrazolium salt [3-(4,5-dimethylthiazol-2-yl)-5-(3-carboxymethoxyphenyl)-2(4-sulfophenyl)-2H-tetrazolium] in MTS to form purple formazan crystals by the dehydrogenase enzymes secreted by mitochondria of metabolically active cells forms the basis of this assay. The formazan dye shows absorbance at 492 nm and the amount of formazan crystals formed is directly proportional to the number of cells. In order to process the samples for the MTS assay, they were rinsed with PBS to remove unattached cells and incubated with 20% MTS reagent in a serum free medium for a period of 3 h at 37°C. Absorbance of the obtained dye was measured at 490 nm using a spectrophotometric plate reader (FLUOstar OPTIMA, BMG lab Technologies).

2.8 Cell morphology

Morphological study of in vitro cultured cardiomyocyte cells on scaffolds was performed after 7 and 14 days of cell culture by processing them for SEM analysis. The scaffolds were rinsed twice with PBS and fixed in 3% glutaraldehyde (Sigma-Aldrich) for 3 h. Thereafter, the scaffolds were rinsed in deionized water and dehydrated with upgrading concentrations of ethanol (50, 70, 90, 100%) twice for 10 min each. Final washing with 100% ethanol was followed by treating the specimens with hexamethyldisilazane (Fluka). The hexamethyldisilazane was air-dried by keeping the samples in fume hood. Finally, the scaffolds were sputter-coated with gold (JEOL JFC-1200 finecoater, Japan) and observed by SEM (FEI-QUANTA 200F, Netherland) at an accelerating voltage of 10 kV.

2.9 Expression of cardiac specific protein marker

Cells cultured on different substrates were fixed using 100% chilled methanol and permeabilized with 0.1% Triton X 100 buffer. The non specific binding sites were blocked using 3% BSA. Thereafter they were stained with anti sarcomeric alpha actinin antibody (Sigma-Aldrich) and FITC (Sigma-Aldrich) as secondary antibody. The nucleus was stained using 4′,6-diamidino-2-phenylindole,DAPI (Invitrogen). Finally, the samples were washed to remove unbound antibodies and mounted using Vectashield (Vector Laboratories). These samples were scanned under Laser Confocal Scanning Microscope (Olympus FV1000) and checked for expression of alpha actinin using Argon laser.

2.10 Statistical analysis

All data are expressed as mean ± standard deviation and were analyzed using Student's *t*-test for the calculation of significance level of the data. Differences were considered statistically significant at $P \leq 0.05$.

3 Results and discussion

3.1 Scaffold fabrication and thermo-mechanical characterization

A commercial P(L)LA-*co*-TMC, containing 30 wt% of TMC, was selected for the preparation of biomimetic electrospun scaffolds for MTE. Thermal characterization of the starting P(L)LA-*co*-TMC (Fig. 1) revealed that the co-polyester is a partially crystalline material that melts at 166°C, with a melting endotherm of 34 J/g. In addition to the melting region, a well defined single glass transition was revealed, at a temperature ($T_g = 33$°C) located between the glass transition temperatures of the respective P(L)LA (T_g around 60°C [49]) and PTMC (T_g between −26 and −15°C, depending on polymer molecular weight [50]) homopolymers, that indicates the presence of a miscible amorphous phase due to the randomness of the copolymer (Fig. 1a). It is noteworthy that during a controlled cooling run from the melt (at 10°C/min) the sample did not crystallize (Fig. 1b) and, upon a subsequent heating run from low temperature, no exothermic peak ascribable to cold crystallization was observed in the experimental conditions

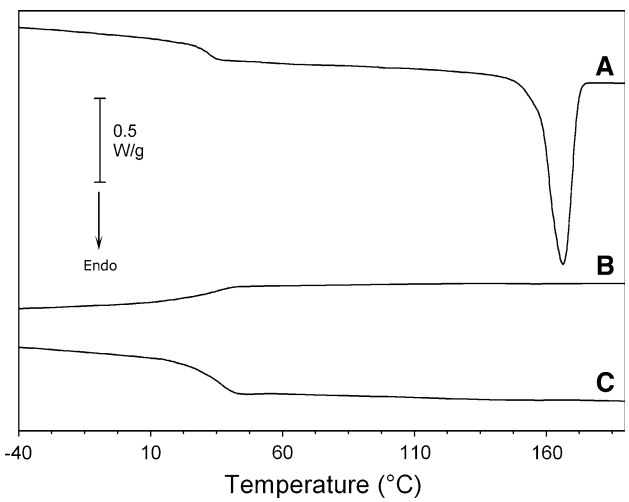

Fig. 1 DSC curves of starting P(L)LA-*co*-TMC: (*a*) first heating scan, (*b*) cooling scan and (*c*) heating scan after cooling from the melt

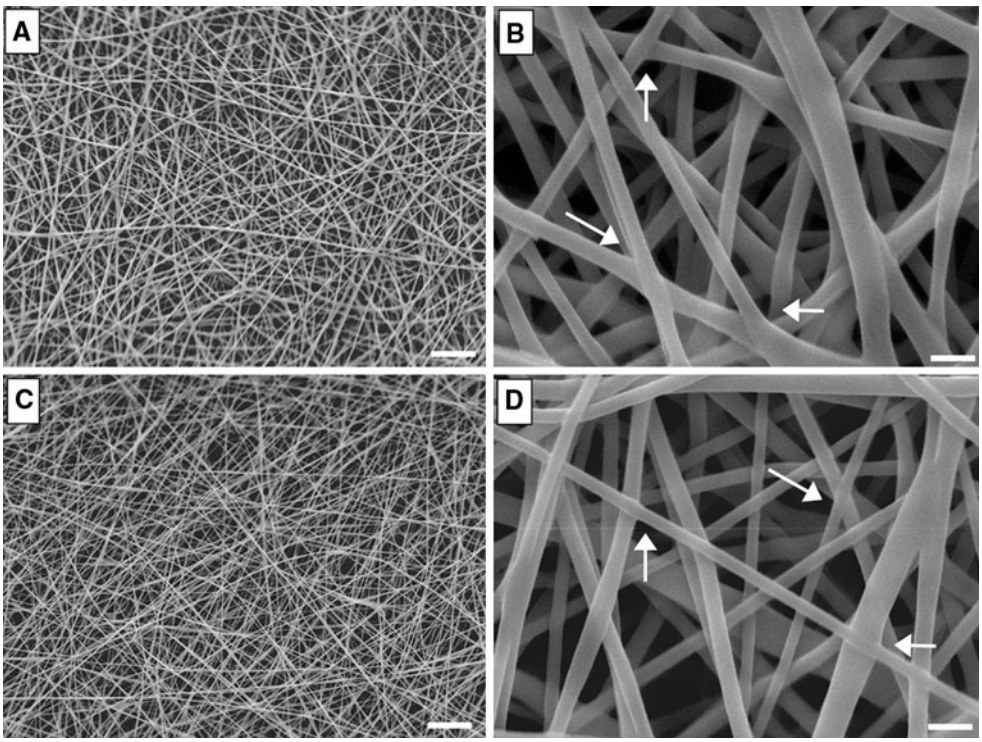

Fig. 2 SEM micrographs of electrospun mats of P(L)LA-*co*-TMC (**a**, **b**) and P(L)LA (**c**, **d**) at two different magnifications. *Arrows* point out fiber-fusion points. Scale *bar* = 20 μm (**a**, **c**); scale *bar* = 2 μm (**b**, **d**)

applied (Fig. 1c). This behavior is attributed to a slow crystallization kinetics of P(L)LA-*co*-TMC. Results of thermal characterization of the P(L)LA-*co*-TMC material used in the present work are in line with earlier data on TMC copolymers with a similar composition synthesized by the group of Albertsson et al. [51].

Highly porous electrospun mats of P(L)LA-*co*-TMC and P(L)LA, with micro-scale interstitial pores and a random orientation of the sub-micrometric fibers were obtained, as revealed by SEM analysis (Fig. 2) (P(L)LA-*co*-TMC mean diameter distribution: 530 ± 110 nm; P(L)LA mean diameter distribution: 610 ± 180 nm). Figure 2 shows that a certain level of 'fiber-fusion' at the contact sites (arrows) was originated during fiber deposition, for both polymers, presumably due to the use of a high boiling point solvent (DMF) during the spinning process. It is pointed out however, that TGA analysis demonstrated the absence of residual solvent in the desiccated electrospun scaffold (data not shown).

Figure 3 shows the DSC curve of the as-spun P(L)LA-*co*-TMC mat and of P(L)LA mat for comparison. The calorimetric analysis revealed the presence of a T_g around 34°C for P(L)LA-*co*-TMC and around 60°C for P(L)LA. DSC curves of both polymers show a cold crystallization exotherm peak followed by a melting endotherm peak of exactly the same entity (P(L)LA-*co*-TMC: $\Delta H_c = \Delta H_m = 17$ J/g; P(L)LA: $\Delta H_c = \Delta H_m = 32$ J/g). This result

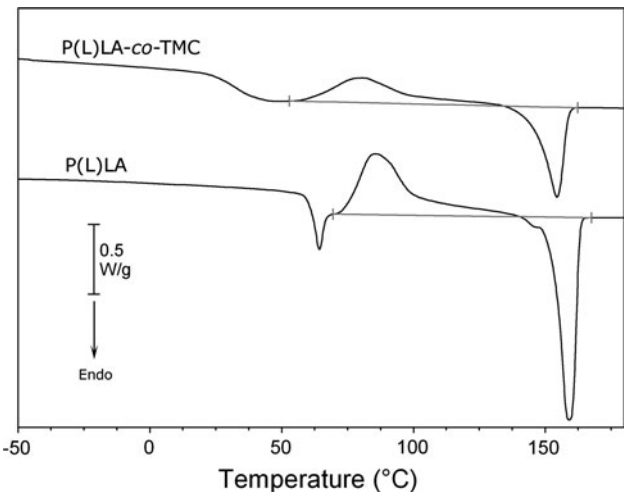

Fig. 3 DSC curves of P(L)LA-*co*-TMC and P(L)LA electrospun mats (first scan, heating rate: 20°C/min)

demonstrates that completely amorphous P(L)LA-*co*-TMC and P(L)LA mats are fabricated through electrospinning since during the process polymer chains have little time to organize in a crystal structure before the occurring of fiber solidification. It is pointed out that, in the case of P(L)LA-*co*-TMC polymer, a certain level of molecular orientation, that is likely originated by the high elongational stretching of the fibers, explains the occurrence of the cold

Table 1 Mechanical properties of P(L)LA-*co*-TMC and P(L)LA electrospun mats measured at RT and at 37°C

Sample	T (°C)	E[a] (MPa)	σ_b[a] (MPa)	ε_b[a] (%)
P(L)LA-*co*-TMC	25	108 ± 10	9.8 ± 2.7	108 ± 16
	37	19 ± 5	8.2 ± 0.6	187 ± 14
P(L)LA	25	105 ± 19	3.4 ± 0.4	101 ± 18
	37	126 ± 25	4.3 ± 0.7	102 ± 13

[a] From stress–strain measurements

E tensile modulus, σ_b stress at break, ε_b strain at break

crystallization phenomena during the DSC heating scan which, on the contrary, did not occur for the starting P(L)LA-*co*-TMC in the form of powder after cooling from the melt, as previously mentioned.

Mechanical performances of electrospun mats were analyzed by tensile stress–strain measurements. It is pointed out that stress–strain data of electrospun materials depend not only on single fiber features but, most of all, on fiber arrangement in the mat and on the presence of 'fiber-fusion' at the contact sites, that remarkably increase the elastic modulus [52]. Moreover, fiber arrangement in the mat is expected to change during the stress–strain measurement. In particular, Lu et al. [53] demonstrated that fibers tend to align in the direction of the applied force before getting thinner and finally breaking. In this work tensile stress–strain analysis of P(L)LA-*co*-TMC non-woven mats were carried out in comparison with electrospun P(L)LA mats of similar thickness, having a fiber diameter distribution comparable to that of P(L)LA-*co*-TMC mat and, similarly to the latter, displaying fiber-fusion at the contact sites (Fig. 2). Table 1 lists mechanical data of the two electrospun materials measured by carrying out stress–strain analysis both at RT and at physiological temperature (37°C), whereas, Fig. 4 reports representative stress–strain curves of both P(L)LA-*co*-TMC and P(L)LA electrospun mats obtained at RT and at 37°C.

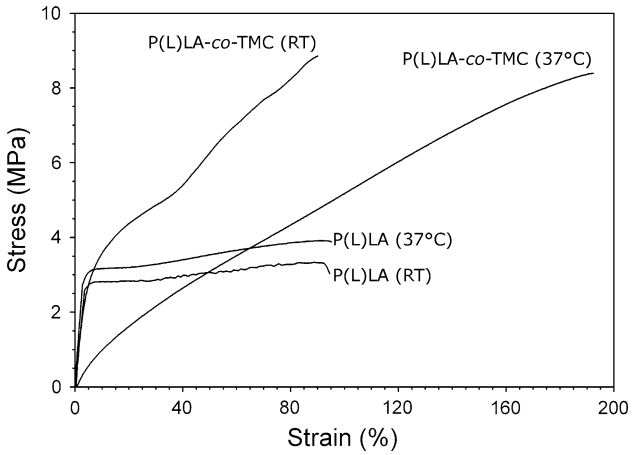

Fig. 4 Stress-strain curves of P(L)LA-*co*-TMC and P(L)LA electrospun mats at RT and 37°C

At RT, comparable elastic moduli were found for P(L)LA and P(L)LA-*co*-TMC. This finding can be justified by the similarity of polymer molecular structures as well as by the fact that fibers of both polymers are completely glassy at RT. Moreover, as stated before, the non-woven structure of the two electrospun mats is similar. The only difference observed is that P(L)LA-*co*-TMC mat is slightly tough than P(L)LA (higher stress at break value). The copolymer, whose tensile strength increases until break, shows a kind of strain hardening behavior, in agreement with previous results obtained by Albertsson et al. on copolymers composed of TMC and (L)LA [54], that might be ascribed to a strain-induced crystallization.

From Fig. 4 and Table 1 it emerges that the mechanical performances of P(L)LA electrospun mat do not change upon temperature increase up to 37°C. On the contrary, the copolymer is considerably more flexible at 37°C, with a lower elastic modulus and a higher deformation at break than at RT. This dramatic change of P(L)LA-*co*-TMC mat mechanical properties is related to the fact that the polymer, being completely amorphous and possessing a T_g around 34°C, is a glassy rigid material at RT while it is a rubbery soft material at 37°C. Therefore, the glass transition at a temperature in between RT and the physiological temperature makes the P(L)LA-*co*-TMC material used in the present work particularly interesting: at RT the polymer can be easily processed through electrospinning into glassy fibers with stable morphology [55], while at physiological conditions it behaves as a soft elastomeric materials.

The elastic properties of the currently investigated materials were evaluated by assessing the ability of the scaffold to recover its initial shape after being deformed to a certain deformation for a short time. To this aim creep-recovery tests were performed at 37°C on P(L)LA-*co*-TMC and on P(L)LA electrospun mats for comparison. Samples were strained to different values of deformation (ε_{in}) by applying, for a period of 2 s, different values of stress and the deformation recovering was recorded as a function of time after removing the stress (Fig. 5). Figure 5a shows that P(L)LA-*co*-TMC mat displays a complete recovery of its initial dimension within 10 s for initial deformations (ε_{in}) lower than 6%. Moreover, when this scaffold is strained at a ε_{in} around 10%, a complete strain-recovery is observed after 2 min from stress removal. Completely different is the creep-recovery response of P(L)LA mat (Fig. 5b) which displays a permanent residual deformation even when it is modestly strained to a deformation of 3%. Mechanical characterization results obtained in the course of this investigation show that the P(L)LA-*co*-TMC material in the form of electrospun mat displays interesting

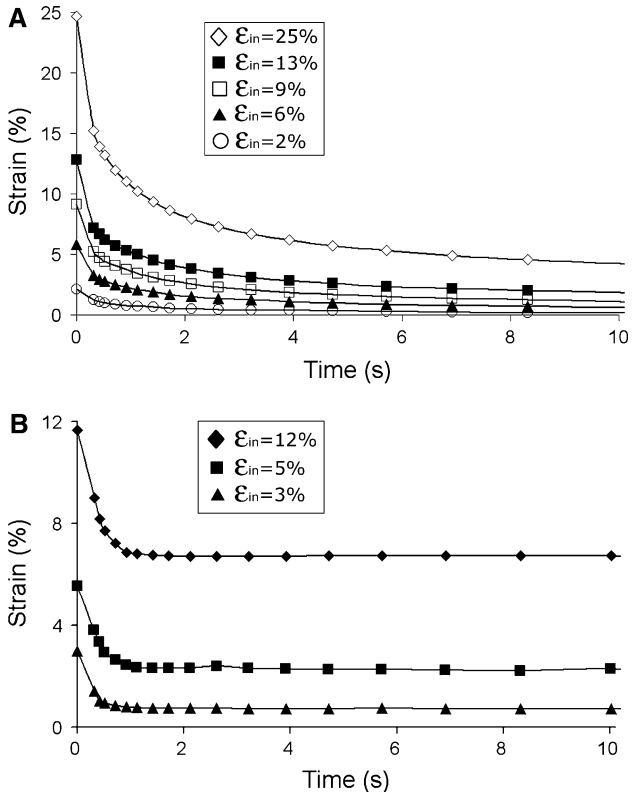

Fig. 5 DMTA creep-recovery experiments on electrospun mats of **a** P(L)LA-*co*-TMC, **b** P(L)LA. Strain-recovery curves for different values of initial maximum strain (ε_{in})

elastomeric behavior, thus it can be considered as a suitable candidate for MTE applications.

3.2 Isolation of cardiomyocytes

Cells isolated from adult rabbit hearts were stained for cardiac specific marker sarcomeric alpha actinin. Cells maintained a rod shape after 1 day of culture in flasks, with clear striations of sarcomeric alpha actinin and troponin T (Fig. 6a). At day 5 few cells were seen to adhere, while the majority of cells still appear to be rod shaped with light striations of sarcomeric alpha actinin and troponin T (Fig. 6b). At day 14, the earlier rod shaped floating cells were no longer observable in the flask. Rather, a monolayer was formed out of the plated cardiac cells containing cardiomyocytes and co-isolated cardiac fibroblasts, which were devoid of their striated appearance. The observation that striations no longer prolonged upon monolayer formation (after day 14, Fig. 6c)—even if cells continued to express alpha actinin—may be attributed to loss of cardiomyocytes myofibril assembly after cell division [56]. The monolayer expressed sarcomeric alpha actinin and troponin T uniformly. These isolated adult cardiac cells were used as a model to understand the cellular interaction with electrospun scaffolds since the mixed cell type represents a more natural myocardium-like environment. Indeed, the myocardium is an ensemble of different cell types embedded in the complex well defined structures of the ECM and arranged in nanoscale topographical and molecular patterns.

3.3 Cell growth and proliferation

Traditionally, a cardiomyocyte is considered terminally differentiated in response to injury. However, recent evidence raises the possibility that a natural system of myocyte repair exists. According to this study, less than 50% of cardiomyocytes are exchanged during a normal life span. Adult hearts have been shown to contain resident stem cells which makes the idea of cardiac regeneration, through ageing and post pathological traumas, plausible [57, 58].

The cytotoxicity of scaffolds and their effect on cell proliferation were studied using the MTS assay. Figure 7 compares the growth profile of isolated cardiomyocytes on P(L)LA-*co*-TMC, P(L)LA and TCP. The growth of cardiomyocytes is always significantly better ($P < 0.05$) at day 14 with respect to day 7. Interestingly, it is evident

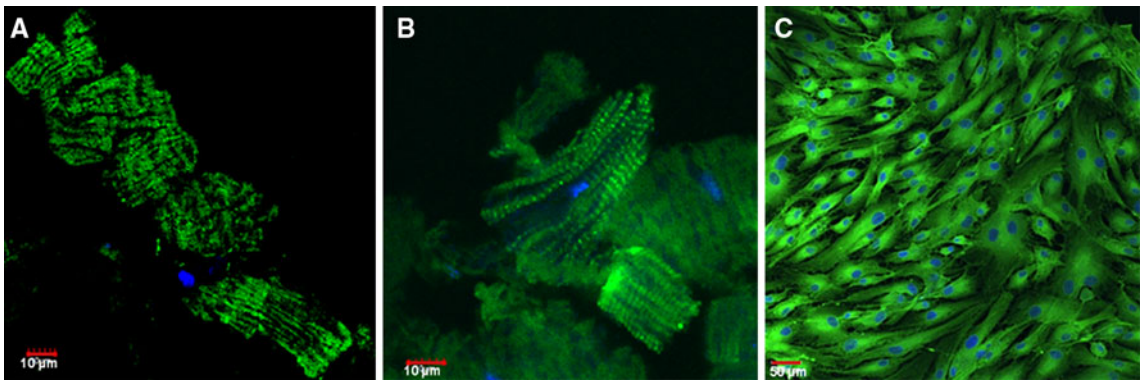

Fig. 6 Freshly isolated cardiomyocytes on TCP stained for sarcomeric alpha actinin at **a** day 1, **b** day 5 and **c** day 14. The expression of alpha actinin is clearly observed in the form of striations (**a** and **b**) which disappear at day 14 (**c**). Scale *bar* = 10 µm (**a**, **b**); scale *bar* = 50 µm (**c**)

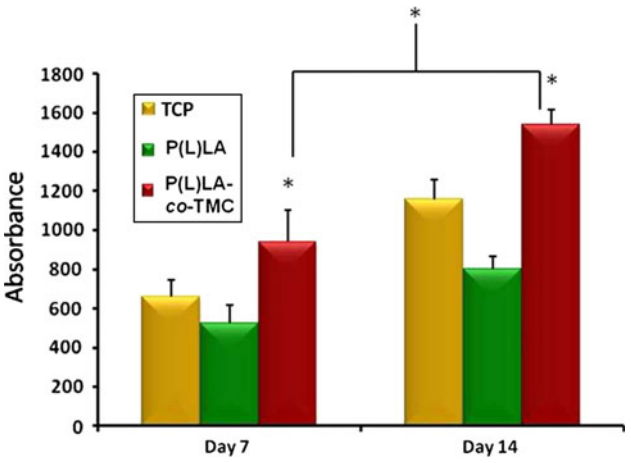

Fig. 7 Cell proliferation assay using MTS. Cardiomyocyte growth at day 7 and day 14 on P(L)LA-*co*-TMC is significantly higher than cell growth on both TCP and P(L)LA. Moreover, a statistically significant difference in cell activity between day 7 and day 14 is observed for P(L)LA-*co*-TMC. (*$P < 0.05$)

from Fig. 7 that at both time points, the growth of cardiomyocytes on P(L)LA-*co*-TMC is significantly higher than the growth on both P(L)LA and TCP ($P < 0.05$). Our results indicate that incorporation of TMC units in P(L)LA macromolecular chain has significant influence on cell growth on nanofibrous scaffolds.

3.4 Cell-material interaction

The interaction of cells with substratum forms the basis of tissue organization. Therefore, in order to explore the potential of our scaffolds in promoting cell-to-cell interaction, we analyzed the different scaffolds at time intervals of 7 and 14 days by means of SEM. Figure 8 depicts the resultant morphological arrangement of cardiomyocytes on P(L)LA-*co*-TMC and P(L)LA at different culture times. It is evident from Fig. 8 that the cells start to stabilize and align themselves by day 14 on P(L)LA-*co*-TMC, whereas on P(L)LA cellular arrangement is rather random and

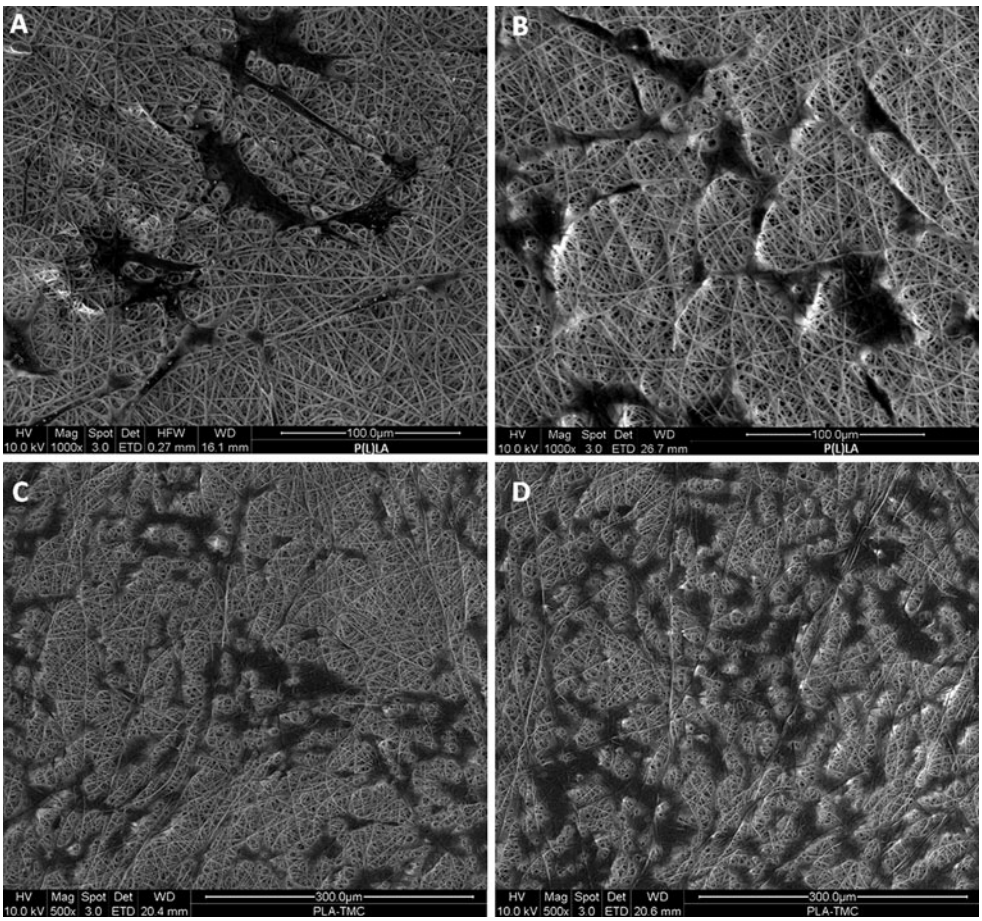

Fig. 8 SEM images of cardiomyocytes grown onto P(L)LA (**a**, **b**) and onto P(L)LA-*co*-TMC (**c**, **d**) after 7 (**a**, **c**) and 14 (**b**, **d**) days of cell culture. Cardiomyocytes cultured onto P(L)LA-*co*-TMC show better cell-to-cell connection indicating superior cellular interaction compared to P(L)LA

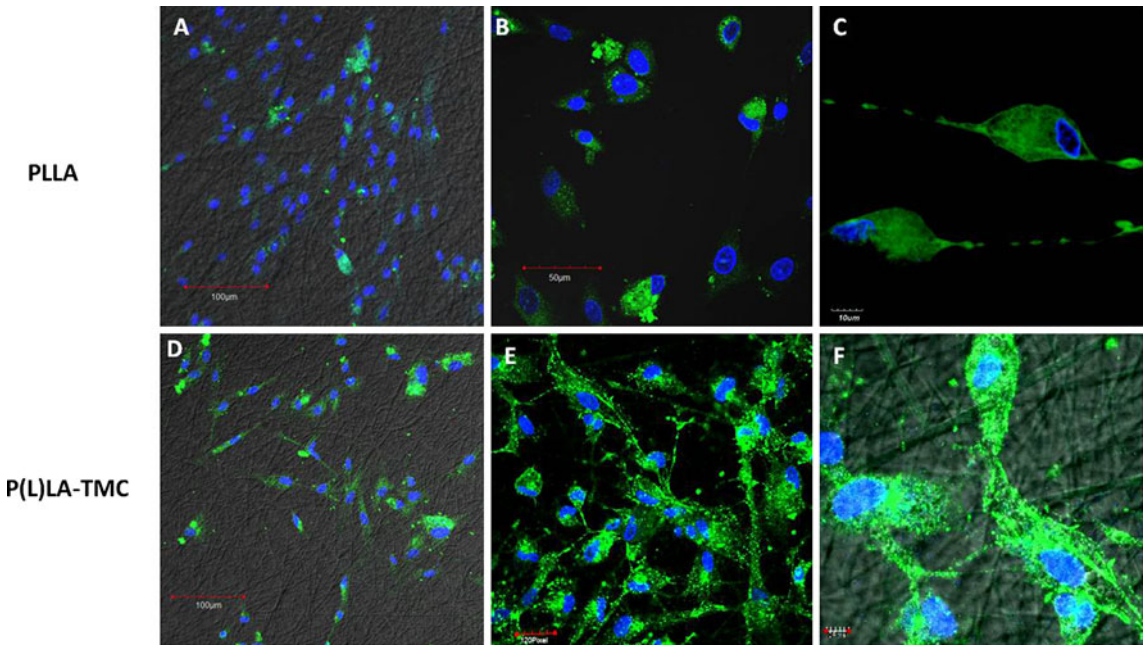

Fig. 9 Immunofluorescence shows cardiomyocytes on random nanofibers of P(L)LA-*co*-TMC and P(L)LA stained for cardiac specific protein sarcomeric alpha actinin at day 14. Cardiomyocytes remain scattered and express alpha actinin in aggregates on P(L)LA (**a**, **b**) and lack fibrillar pattern (**c**). However, P(L)LA-*co*-TMC shows intense expression of alpha actinin and cell–cell and cell–material interaction (**d**, **e**). Cells on P(L)LA-*co*-TMC show re-appearance of fibrillar pattern of alpha actinin expression (**f**)

scattered. In particular, by day 14, P(L)LA-*co*-TMC shows formation of cardiomyocyte monolayer interconnected by intercellular junctions that are well aligned and guided in evidently parallel fashion. The intercellular network on P(L)LA-*co*-TMC was also observed to be superior to that on TCP on day 14 (data not shown). These results indicate that P(L)LA-*co*-TMC provides better adhesion at a nanoscale level than P(L)LA.

From a clinical perspective, it is of utmost importance that an implantable material integrates with the host organ cells and this is initiated in the form of cell spreading. The latter is also indicative of acceptance from the host. The inability of a biomaterial to promote cell spreading and integration limits its use at clinical level [59]. Lack of suitable microenvironment in myocardium post MI is the main cause of cell loss in cellular therapeutics. Our results confirm that P(L)LA-*co*-TMC provides a suitable microenvironment where cells can interact well with other cells as well as with the nanofibrous scaffold.

Growth and morphology of cells is largely associated with their normal functioning. These functions include expression of characteristic proteins. To elucidate the effect of the different substrates, we studied the expression of the characteristic protein marker, sarcomeric alpha actinin, in the cardiomyocytes grown onto the scaffolds. Alpha actinin is an actin cross-linking protein that cross-links two filaments of actin [60]. Our results show differences in the expression patterns of alpha actinin in cardiomyocytes grown onto P(L)LA-*co*-TMC and P(L)LA. Figure 9c, d shows expression of alpha actinin in cardiomyocytes on P(L)LA-*co*-TMC in the form of reformed striations. Such striations were seen on newly isolated cardiomyocytes only up to 5 days of culture (Fig. 6a, b) while at day 14 the striated appearance of alpha actinin expression on TCP was not observed (Fig. 6c). Cells grown onto P(L)LA lack such striated appearance (Fig. 9a, b) indicating that cardiomyocyte growth is functionally enhanced on P(L)LA-*co*-TMC. Thus, our results indicate that nanofibers of P(L)LA-*co*-TMC not only aid in integrating cells with biomaterial but also maintain normal morphology and functioning of cardiomyocytes.

4 Conclusion

We successfully fabricated nanofibrous scaffolds of P(L)LA-*co*-TMC and we demonstrated that the introduction of TMC units in P(L)LA chain confers elastomeric properties to the material and enhance cardiomyocyte proliferation, cell morphology preservation and expression of cardiac marker protein alpha actinin. Indeed, P(L)LA-*co*-TMC has a lower glass transition temperature compared to P(L)LA homopolymer and displays an elastic behavior at 37°C, with an elastic modulus a magnitude nearing to that of native heart tissue, making this polymer attractive for myocardial regeneration. This is supported by enhanced

proliferation of cardiomyocytes isolated from adult heart that preserve their ability to develop intercellular interactions and impressively maintain morphology and expression of cardiac protein markers in the form of striations. Thus, our results indicate that electrospun P(L)LA-*co*-TMC performs excellently as a scaffold for cardiomyocytes, and it is a highly potential synthetic biomaterial for MTE.

Acknowledgments The authors gratefully acknowledge the NRF-Technion (Grant No.: R-398-001-063-592), Division of Bioengineering, Nanoscience and Nanotechnology Initiative (National University of Singapore) and Italian Ministry of University and Research for the financial support. C.G. is the recipient of a fellowship awarded from the Spinner Consortium of Regione Emilia Romagna (Italy).

References

1. Kao RL, Browder W, Li C. Cellular cardiomyoplasty: What have we learned? Asian Cardiov Thorac Ann. 2009;17:89–101.
2. Kong HJ, Kaigler D, Kim K, Mooney DJ. Controlling rigidity and degradation of alginate hydrogels via molecular weight distribution. Biomacromolecules. 2004;5:1720–7.
3. Serrano MC, Chung EJ, Ameer GA. Advances and applications of biodegradable elastomers in regenerative medicine. Adv Func Mat. 2010;20:192–208.
4. Omens JH. Stress and strain as regulators of myocardial growth. Prog Biophys Mol Biol. 1998;69:559–72.
5. Nagueh SF, Shah G, Wu Y, Lahmers S. Altered titin expression, myocardial stiffness, and left ventricular function in patients with dilated cardiomyopathy. Circulation. 2004;110:155–62.
6. Mukherjee S, Venugopal J, Ravichandran R, Ramakrishna S, Raghunath M. Multimodal biomaterial strategies for regeneration of infarcted myocardium. J Mater Chem. 2010;20:8819–31.
7. Eschenhagen T, Didié M, Munzel F, Schubert P, Zimmerman W-H. 3D engineered heart tissue for replacement therapy. Bas Res Cardiol. 2002;97:146–52.
8. Chiu LLY, Radisic M, Vujak-Novakovic G. Bioactive scaffolds for engineering vascularized cardiac tissues. Macromol Biosci. 2010;10:1286–301.
9. Kofidis T, Akhyari P, Boublik J, Theodorou P, Martin U, Ruhparwar A, Fischer S, Eschenhagen T, Kubis HP, Kraft T, Leyh R, Haverich A. In vitro engineering of heart muscle: artificial myocardial tissue. J Thor Cardiovasc Surg. 2002;124:63–9.
10. Kofidis T, de Bruin JL, Hoyt G, Ho Y, Tanaka M, Yamane T, Lebl DR, Swijnenburg R-J, Chang C-P, Quertermous T, Robbins RC. Myocardial restoration with embryonic stem cell bioartificial tissue transplantation. J Heart Lung Transpl. 2005;24(6):737–44.
11. Zimmerman W-H, Fink C, Kralish D, Remmers U, Weil J, Eschenhagen T. Three-dimensional engineered heart tissue from neonatal rat cardiac myocytes. Biotechnol Bioeng. 2000;68:106–14.
12. Amir G, Miller L, Shachar M, Feinberg MS, Holbova R, Cohen S, Leor J. Evaluation of a peritoneal-generated cardiac patch in a rat model of heterotopic heart transplantation. Cell Transpl. 2009;18:275–82.
13. Ayelet D, Shachar M, Leor J, Cohen S. Cardiac tissue engineering-optimization of cardiac cell seeding and distribution in 3D porous alginate scaffolds. Biotechnol Bioeng. 2002;80:305–12.
14. Leor J, Aboulafia-Etzion S, Ayelet D, Shapiro L, Barbash IM, Battler A, Granot J, Cohen S. Bioengineered cardiac grafts: a new approach to repair the infarcted myocardium. Circulation. 2000;102:56–61.
15. Sapir Y, Kryukov O, Cohen S. Integration of multiple cell–matrix interactions into alginate scaffolds for promoting cardiac tissue regeneration. Biomaterials. 2011;32:1838–47.
16. Akhyari P, Fedak PWM, Weisel RD, Lee T-YJ, Verma S, Mickle DAG, Li R-K. Mechanical stretch regimen enhances the formation of bioengineered autologous cardiac muscle graft. Circulation. 2002;106:137–42.
17. Iwakura A, Fujita M, Kataoka K, Tambara K, Sakakibara Y, Komeda M, Tabada Y. Intramyocardial sustained delivery of basic fibroblast growth factor improves angiogenesis and ventricular function in a rat infarct model. Heart Vessel. 2003;18:93–9.
18. Lutolf MP, Hubbell JA. Synthetic biomaterials as instructive extracellular microenvironments for morphogenesis in tissue engineering. Nat Biotechnol. 2005;23:47–55.
19. Williams DF. On the nature of biomaterials. Biomaterials. 2009;30:5897–909.
20. Bursac N, Papadaki M, Cohen RJ, Schoen FJ, Eisenberg SR, Carrier R, Vujak-Novakovic G, Freed LE. Cardiac muscle tissue engineering: toward an in vitro model for electrophysiological studies. Am J Physiol. 1999;277:433–44.
21. Hosseinkhani H, Hosseinkhani M, Hattori S, Matsuoka R, Kawaguchi N. Micro and nano-scale in vitro 3D culture system for cardiac stem cells. J Biomed Mat Res. 2010;94A:1–8.
22. Ke Q, Yang Y, Rana JS, Yu C, Morgan JP, Yong-Fu X. Embryonic stem cells cultured in biodegradable scaffold repair infarcted myocardium in mice. Acta Physiol Sin. 2005;57:673–81.
23. Kellar RS, Landeen LK, Shephered BR, Naughton GK, Ratcliffe A, Williams SK. Scaffold-based three-dimensional human fibroblast culture provides a structural matrix that supports angiogenesis in infarcted heart tissue. Circulation. 2001;104:2063–8.
24. Rabkin E, Schoen J. Cardiovascular tissue engineering. Cardiovasc Pathol. 2002;11:305–17.
25. Alperin C, Zandstra PW, Woodhouse KA. Polyurethane films seeded with embryonic stem cell-derived cardiomyocytes for use in cardiac tissue engineering applications. Biomaterials. 2005;26:7377–86.
26. Giraud M-N, Flueckiger R, Cook S, Ayuni E, Siepe M, Carrel T, Tevaearai HT. Long-term evaluation of myoblast seeded patches implanted on infarcted rat hearts. Artif Organs. 2010;34:E184–92.
27. McDevitt TC, Woodhouse KA, Hauschka SD, Murry CE, Stayton PS. Spatially organized layers of cardiomyocytes on biodegradable polyurethane films for myocardial repair. J Biomed Mat Res. 2003;66A:586–95.
28. Siepe M, Giraud M-N, Liljensten E, Nydegger U, Menasche P, Carrel T, Tevaearai HT. Construction of skeletal myoblast-based polyurethane scaffolds for myocardial repair. Artif Organs. 2007;31:425–33.
29. Krupnick AS, Kreisel D, Engels FH, Szeto WY, Plappert T, Pompa SH, Flake AW, Rosengard BR. A novel small animal model of left ventricular tissue engineering. J Heart Lung Transpl. 2002;21:233–43.
30. Ozawa T, Mickle DAG, Weisel RD, Koyama N, Ozawa S, Li R-K. Optimal biomaterial for creation of autologous cardiac grafts. Circulation. 2002;106:176–82.
31. Park H, Radisic M, Lim JO, Chang BH, Vujak-Novakovic G. A novel composite scaffold for cardiac tissue engineering. In Vitro Cell Dev Biol Anim. 2005;41:188–96.
32. Bat E, van Kooten TG, Feijen J, Grijpma DW. Resorbable elastomeric networks prepared by photocrosslinking of high-molecular-weight poly(trimethylene carbonate) with photoinitiators and

poly(trimethylene carbonate) macromers as crosslinking aids. Acta Biomater. 2011;7:1939–48.
33. Bruggeman JP, de Bruin B-J, Bettinger CJ, Langer R. Biodegradable poly(polyol sebacate) polymers. Biomaterials. 2008;29:4726–35.
34. Chen Q-Z, Bismarck A, Hansen U, Junaid S, Tran MQ, Harding SE, Ali NN, Boccaccini AR. Characterization of a soft elastomer poly(glycerol sebacate) designed to match the mechanical propeeties of myocardial tissue. Biomaterials. 2008;29:47–57.
35. Song Y, Kamphuis MMJ, Zhang Z, LMTh Sterk, Poot AA, Feijen J, Grijpma DW. Flexible and elastic porous poly(trimethylene carbonate) structures for use in vascular tissue engineering. Acta Biomater. 2010;6:1269–77.
36. Wang Y, Ameer GA, Sheppard B, Langer R. A tough biodegradable elastomer. Nat Biotechnol. 2002;20:602–6.
37. You Z, Cao H, Gao J, Shin PH, Day BW, Wang Y. A functionalizable polyester with free hydroxyl groups and tunable physiochemical and biological properties. Biomaterials. 2010;31:3129–38.
38. Buchholz B. Analysis and characterization of resorbable D,L-lactide-trimethylene carbonate copolyesters. J Mat Sci: Mat Med. 1993;4:381–8.
39. Pego AP, Poot AA, Grijpma DW, Feijen J. Physical properties of high molecular weight 1,3-trimethylene carbonate and D,L-lactide copolymers. J Mater Sci: Mater Med. 2003;14:767–73.
40. Tyson T, Finne-Wistrand A, Albertsson A-C. Degradable porous scaffolds from various L-lactide and trimethylene carbonate copolymers obtained by a simple and effective method. Biomacromolecules. 2009;10:149–54.
41. Pego AP, Siebum B, Luyn V, Gallego XJ, Seijen YV, Poot AA, Grijpma DW, Feijen J. Preparation of degradable porous structures based on 1,3-trimethylene carbonate and D,L-lactide (co)polymers for heart tissue engineering. Tissue Eng. 2003;9:981–94.
42. Pego AP, Poot AA, Grijpma DW, Feijen J. Biodegradable elastomeric scaffolds for soft tissue engineering. J Control Release. 2003;87:69–79.
43. Pego AP, Van Luyn MJA, Brouwer LA, Van Wachem PB, Poot AA, Grijpma DW, Feijen J. In vivo behavior of poly(1,3-trimethylene carbonate) and copolymers of 1,3-trimethylene carbonate with D,L-lactide or -caprolactone: degradation and tissue response. J Biomed Mater Res. 2003;67A:1044–54.
44. Li M, Mondrinos MJ, Chen X, Gandhi MR, Ko FK, Lelkes PI. Co-electrospun poly(lactide-co-glycolide), gelatin and elastin blends for tissue engineering scaffolds. J Biomed Mater Res. 2006;79A:963–73.
45. Rockwood DN, REJr Akins, Parrag IC, Woodhouse KA, Rabolt JF. Culture on electrospun polyurethane scaffolds decreases atrial natriuretic peptide expression by cardiomyocytes in vitro. Biomaterials. 2008;29:4783–91.
46. Shin M, Ishii O, Sueda T, Vacanti JP. Contractile cardiac grafts using a novel nanofibrous mesh. Biomaterials. 2004;25:3717–23.
47. Stankus JJ, Guan J, Wagner WR. Fabrication of biodegradable elastomeric scaffolds with sub-micron morphologies. J Biomed Mater Res. 2004;70A:603–14.
48. Zong X, Bien H, Chung CY, Yin L, Fang D, Hsiao BS, Chu B, Entcheva E. Electrospun fine-textured scaffolds for heart tissue constructs. Biomaterials. 2005;26:5330–8.
49. Gupta B, Revagade N, Hilborn J. Poly(lactic acid) fiber: an overview. Prog Polym Sci. 2007;32:455–82.
50. Zhu KJ, Hendren RW, Jensen K, Pitt CG. Synthesis, properties, and biodegradation of poly(1,3-trimethylene carbonate). Macromolecules. 1991;24:1736–40.
51. Peter P, Malberg S, Albertsson AC. Design of resorbable porous tubular copolyester scaffolds for use in nerve regeneration. Biomacromolecules. 2009;10:1259–64.
52. Wei X, Xia Z, Wong S-C, Baji A. Modelling of mechanical peroperties of electrospun nanofibre network. Int J Exp Comput Biomech. 2009;1:45–57.
53. Lu J-W, Zhang ZP, Ren XZ, Chen YZ, Yu J, Guo ZX. High-elongation fiber mats by electrospinning of polyoxymethylene. Macromolecules. 2008;41:3762–4.
54. Andronova N, Albertsson A-C. Resilient bioresorbable copolymers based on trimethylene carbonate, L-lactide, and 1,5-dioxepan-2-one. Biomacromolecules. 2006;7:1495.
55. Focarete ML, Gualandi C, Moroni L. Working with electrospun scaffolds: some practical hints for tissue engineers. In: Haghi AK, editor. Electrospun nanofibers research: recent developments, Hauppauge. New York: Nova Science Publisher; 2009. p. 19–34.
56. Du A, Sanger JM, Linask KK, Sanger JW. Myofibrillogenesis in the first cardiomyocytes formed from isolated quail precardiac mesoderm. Dev Biol. 2003;257:382–94.
57. Messina E, De Angelis L, Frati G, Morrone S, Chimenti S, Fiordaliso F, Salio M, Battaglia M, Latronico MV, Coletta M, Vivarelli E, Frati L, Cossu G, Giacomello A. Isolation and expansion of adult cardiac stem cells from human and murine heart. Circ Res. 2004;95:911–21.
58. Bearzi C, Rota M, Hosoda T, Tillmanns J, Nacimbene A, De Angelis A, Yasuzawa-Amano S, Trofimova I, Siggins RW, LeCapitaine N, Cascapera S, Beltrami AP, D'Alessandro DA, Zias E, Quaini F, Urbanek K, Michler RE, Bolli R, Kajstura J, Leri A, Anversa P. Human cardiac stem cells. Proc Natl Acad Sci USA. 2007;104:14068–73.
59. Martinez EC, Kofidis T. Myocardial tissue engineering: the quest for the ideal myocardial substitute. Expert Rev Cardiovasc Ther. 2009;7:921–8.
60. Cabello N, Remelli R, Canela L, Soriguera A, Mallol J, Canela EI, Robbins MJ, Lluis C, Franco R, McIlhinney RA, Ciruela F. Actin-binding protein alpha-actinin-1 interacts with the metabotropic glutamate receptor type 5b and modulates the cell surface expression and function of the receptor. J Biol Chem. 2007;282:12143–53.